34th Annual International Conference of the IEEE EMBS
San Diego, California USA, 28 August - 1 September, 2012

Towards More Precise, Minimally-Invasive Tumour Treatment Under Free Breathing

Frank Preiswerk, Patrik Arnold, Beat Fasel and Philippe C. Cattin[1]

***Abstract*— In recent years, significant advances have been made towards compensating respiratory organ motion for the treatment of tumours, *e.g.* for the liver. Among the most promising approaches are statistical population models of organ motion.**

In this paper we give an overview on our work in the field. We explain how 4D motion data can be acquired, how these motion models can then be built and applied in realistic scenarios. The application of the motion models is first shown on a case where 3D surrogate marker data is available. Then we will evaluate the prediction accuracy if only 2D and lastly 1D surrogate marker motion data is available. For all three scenarios we will give quantitative prediction accuracy results.

I. INTRODUCTION

Respiratory organ motion is a complicating factor in the treatment of liver tumours. Non-rigid deformation during breathing introduces a significant amount of uncertainty in location during irradiation of a tumour. It has been shown that 4D treatment planning is important for improved precision in radiotherapy [10]. A lot of research has been done for handling respiratory motion of organs. Some of the approaches rely on a correlation between external markers and internal organ motion [5], which is not always valid either due to organ drift [12], [6] or because of varying motion patterns at different positions of the organ. The approach by Ehrhardt *et al.* [4] is mathematically well formulated but requires quite a few assumptions about breathing-depth and voxel intensities and falls short in the temporal resolution of the model. Our approach to this problem is based on the acquisition of Magnetic Resonance Imaging (MRI) sequences of volunteers and a number of algorithms for processing this data. First, we retrospectively reconstruct 4D images in order to generate a 4D-MRI sequence for each subject. Then we register the data to obtain deformation fields for each sequence and establish mechanical correspondence among all subjects. We finally capture the motion information by learning a PCA model of the deviation from exhalation position during quiet breathing. Finally, we apply a prediction algorithm to sparse data in order to obtain a reconstruction of the motion for the whole organ at any point in time. Our model can equally well handle 1D, 2D or 3D input information. Even if only a single 1D signal (*i.e.* the Superior/Inferior (SI) motion component of a single point on the diaphragm) is available, our model provides an accurate reconstruction of the position of the complete organ.

In this paper we shortly wrap up the basics of our modeling pipeline. We provide quantitative results of two of our most recent studies and additionally give the latest results on using our model in a gated setting with only a 1D surrogate.

[1]Medical Image Analysis Center, University of Basel, Switzerland
frank.preiswerk at unibas.ch

II. STATISTICAL MOTION MODEL

Building a statistical motion model comprises of a number of steps. First, the image data is obtained using an MRI scanner and the data is registered to obtain deformation fields over time. Then, correspondence is established among all subjects. Finally, the deformation fields are processed using Principal Component Analysis (PCA) to compute the model.

A. Data Acquisition

We used 4D-MRI sequences [11] of the liver from 20 healthy subjects. The in-plane resolution is in the range of 1.5 mm and the slice thickness is $3-4$ mm, depending on the subject. The data was acquired over roughly one hour on 22 to 30 sagittal slices and a temporal resolution of $2.6-2.8$ Hz. 4D-MRI sequences are generated by retrospectively stacking the acquired 2D image slices based on the navigator technique as described in [11], and depicted in Fig. 1.

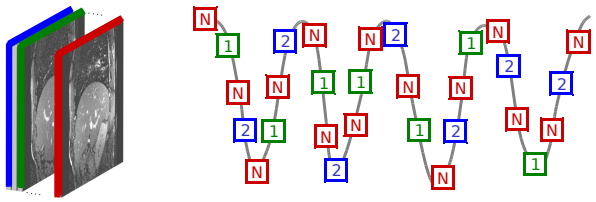

Fig. 1. The 4D-MRI acquisition scheme. Each slice position $(1, 2, \ldots)$ is temporally encapsulated by two navigators (N). The navigator slice is always acquired at the same spatial position and defines a phase for each encapsulated image. This allows to find matching slices of the same breathing phase for each position and thus gives a 3D stack for every point in time.

The 3D deformation fields are then extracted using the B-spline based non-rigid registration method proposed by Rueckert *et al.* [9]. This process involved the manual segmentation of the liver in one master exhalation stack for each subject and results in dense deformation fields between this exhalation master and all respiratory states, see Fig. 2.

B. Establishment of Correspondence

In order to build a statistical model from the deformation fields, inter-subject correspondence has to be established. We developed a correspondence scheme that makes it easy to apply the model to a new subject [8]. In a preparatory step, the liver of each subject was manually segmented on each

978-1-4577-1787-1/12/$26.00 ©2012 IEEE

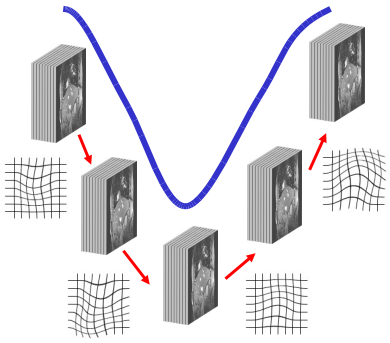

Fig. 2. Non-ririd registration of the 4D-MRI stacks results in dense spatio-temporal motionfields.

(a) (b) (c)

Fig. 3. (a) Manually selected landmarks for correspondence on a selected sagittal slice. (b) Manually defined mask. (c) Automatically generated re-sampling of the liver contour based on mask and landmarks. The alternating markers highlight the four individually controlled segments.

sagittal slice of one MRI scan. Additionally, four points were manually selected on each slice to define the correspondence: Two points where the liver is attached to the anterior and posterior wall, respectively, as well as the highest point on the superior end (diaphragm) and the lowest point at the inferior end of the organ, see Fig. 3(a). We applied an arc-length discretisation algorithm that combines the mask and landmarks to resample the organ contour for each slice, see Fig. 3(b)&3(c). The data is then again resampled in z-direction because image acquisitions of different subjects can consist of different numbers of slices. In order to establish correspondence for points within the liver, an isotropic grid was placed in the average liver and then transformed to each of the remeshed surfaces using the Delaunay tetrahedrisation approach [2], see Fig. 4. This finally gave a set of 20 topologically equivalent 3D liver volumes that constitute one exhalation master $\hat{\mathbf{v}}$ for each subject and combined with the registration results, dense spatio-temporal motion fields for each grid point.

C. Statistical Model and Reconstruction

In our statistical model, a liver instance is represented by a $3n$-dimensional vector $\mathbf{v} = (x_1, y_1, z_1, \dots, x_n, y_n, z_n)$, where n corresponds to the number of model vertices. After removing the shape information by taking the vector-field difference between each respiratory state $\mathbf{v}$ and the subject's exhalation master state $\check{\mathbf{v}}$, we get the motion data that is used

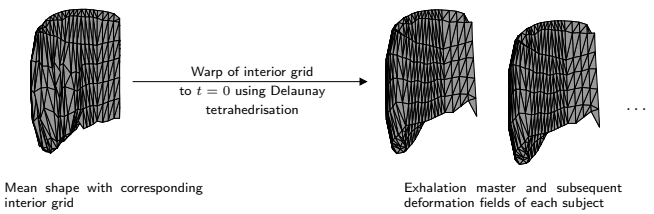

Fig. 4. An isotropic grid is positioned inside the mean shape and warped to the exhalation master shape $\check{\mathbf{v}}$ at $t = 0$ of each subject. From $t = 0$ to all forthcoming time steps, the deformation field is used to further warp the grid to any of the subsequent respiratory steps. This results in dense intra- and inter-subject correspondence.

to build the model: $\mathbf{x} = \mathbf{v} - \check{\mathbf{v}}$. Principal Component Analysis (PCA) on all samples $\mathbf{X} = (\mathbf{x}_1, \dots, \mathbf{x}_m)$ yields the orthonormal matrix of principal components $\mathbf{U} = (\mathbf{u}_1, \dots, \mathbf{u}_{m-1})$ and their corresponding Eigenvalues $\lambda_1, \dots, \lambda_{m-1}$ that represent the standard deviation σ_i of the principal components in descending order ($\sqrt{\lambda_i} = \sigma_i$). We can transform (and thus decorrelate) the data by subtracting the mean offset vector $\mu = \frac{1}{m} \sum \mathbf{x}_i$, followed by a projection into model space:

$$\mathbf{c} = \mathrm{diag}(\sigma_i^{-1}) \mathbf{U}^T (\mathbf{x} - \mu)\,, \tag{1}$$

The deviation of a liver shape from its exhalation position during respiration can now be described in terms of our model,

$$\mathbf{v} = \check{\mathbf{v}} + \mathrm{diag}(\sigma_i) \mathbf{U} \mathbf{c} + \mu\,. \tag{2}$$

From the observed partial information, we have to estimate a suitable model coefficient vector $\mathbf{c}$ that represents the motion information of the whole liver. In practice, this information may come, for example, from structures tracked in ultrasound, x-ray or portal images or from implanted electromagnetic beacons. We use the approach described in [3] to solve this problem. The partial observations are given by the vector $\mathbf{r} = \mathbf{L}(\mathbf{x} - \mu)$, with a mapping $\mathbf{L} : \mathbb{R}^n \rightarrow \mathbb{R}^l, l < n$. Our aim is to find the model coefficient $\mathbf{c}$ for the full vector $\mathbf{x}$ that describes our partial measurement. As we cannot expect to find an exact solution, we define the best reconstruction to be the one with minimal Mahalanobis distance $||\mathbf{c}||^2$, *i.e.* the one with highest prior probability. This can be formulated as a minimisation problem with regard to the model coefficients,

$$E = ||\mathbf{Q}\mathbf{c} - \mathbf{r}||^2 + \eta \cdot ||\mathbf{c}||^2\,, \tag{3}$$

with $\mathbf{Q} = \mathbf{L}\mathbf{U} \cdot \mathrm{diag}(\sigma_i)$. The regularisation factor η allows to trade off matching quality against prior probability. From the singular value decomposition $\mathbf{Q} = \overline{\mathbf{V}}\mathbf{W}\mathbf{V}^T$ we can calculate the most probable coefficients in a Bayesian sense,

$$\mathbf{c} = \mathbf{V}\, \mathrm{diag}\left(\frac{w_i}{w_i^2 + \eta}\right) \overline{\mathbf{V}}^T \mathbf{r}\,. \tag{4}$$

The final shape can then be computed by projecting the model coefficient $\mathbf{c}$ back into spatial domain according to Eq. (2). Note that $\mathbf{Q}$ is of size $l \times \hat{m}$, with $\hat{m} \ll m$ the number of principal components used for reconstruction. Therefore, Eq. (4) can be easily solved in real-time.

III. Experiments

Given the statistical motion model, it can be applied for predicting the tumour location from surrogate markers. In the following we first evaluate our model when a set of 3D surrogate markers is available. Then we progressively increase the difficulty by predicting only based on 2D surrogate marker information and lastly based on a simple 1D signal.

A. Prediction from Sparse 3D Data

In the first scenario [7] we assume that surrogate markers can be tracked in three dimensions. This scenario is applicable to a treatment *e.g.* with the Calypso System (Calypso Medical Technologies, Inc) which provides accurate real-time 3D positions of implanted markers. Similar data can also be produced by bi-plane X-rays such as in the CyberKnife Robotic Radiosurgery System (Accuray, Inc.). We obtained an average error of $1.2\ \mathrm{mm}$. Furthermore, the 95^{th} percentile of the errors was at $2.8\ \mathrm{mm}$ and the large errors appeared mainly at inhalation. This suggests that the error could be additionally reduced using amplitude gating, where no prediction (and thus no treatment) is performed near full inhalation, see Fig. 8

B. Prediction from Sparse 2D Data under Projection and Noise

In the next scenario we evaluated the motion models in a set-up where only 2D motion information is available [8]. Clinically, this applies to cases where ultrasound or portal images are used to observe the organ during treatment. We simulated such 2D data by projecting the 3D positions to 2D planes under a large number of different projection angles and additionally superimposed Gaussian noise ($\sigma = 2\ \mathrm{mm}$) in order to simulate for various sources of errors that would arise in a real-world setup. The model is able to accurately predict the overall 3D deformation field, similarly to the case where 3D surrogate information is available. Our method is sufficiently robust to produce accurate reconstructions even in presence of noise. For the sagittal view, we obtained an average error of $2.6\ \mathrm{mm}$. Figure 5 clearly shows that this error depends on the projection angle (the sagittal view was defined to be at position $[0, 0]$). The reason for this being that the SI motion is not visible in near-axial projections. The figure also suggests that there is a certain tolerance to deviate from a perfectly sagittal viewing angle without significantly sacrificing prediction accuracy. This, of course, is an important insight for practical applications where such parameters cannot be chosen freely.

C. Prediction from 1D and 2D Data with Amplitude Gating

In the last scenario we aim at compensating the organ motion for an MR-guided HIFU system under free breathing. As the MR system is used for temperature mapping of the HIFU ablation process, no or only little scan time can be used to track the tumour. In this scenario we thus evaluated the prediction power assuming that the diaphragm can either be tracked with an additional MR-compatible 2D ultrasound probe or using a simple and fast pencil beam located on the diaphragm [1]. We applied normalised cross correlation to track one point on the diaphragm over time. Our prediction algorithm is then driven by this offset, which gives a complete 3D position for the liver at every point in time. Figure 6 depicts the navigator slice of one subject together with the tracked positions of the diaphragm. We extracted this data for each subject and obtained results for continuous prediction as shown in Figure 7. The plot shows results for 1D, 2D and 3D predictions. Table I summarise the numbers. In the 1D case we only used the SI component of the signal, which characterises the main mode of motion for the liver. Using two components improves the result slightly. In the 3D case, we used the actual 3D position of the surrogate instead of the tracking results, as in Section III-A. The results show that our model can be used even in cases where only a 1D signal is available, *e.g.* from a respiration belt or an optical tracker, although one has to keep in mind that external signals do not always correlate sufficiently with internal motion [12].

We combined our model-based approach with respiratory gating in order to additionally reduce the prediction error.

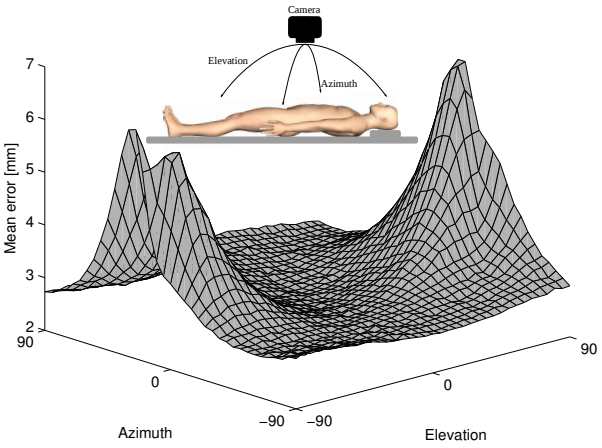

Fig. 5. This surface shows the mean error over all subjects as a function of the camera position. It can be nicely seen that the prediction accuracy drops significantly when el approaches the values $+90°$ and $-90°$.

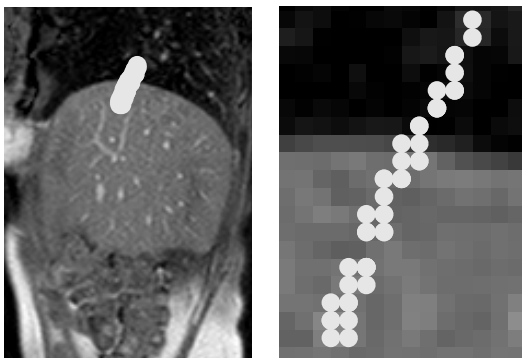

(a) (b)

Fig. 6. Selection of tracked organ position using template matching that were used as input for prediction (a), close-up view (b).

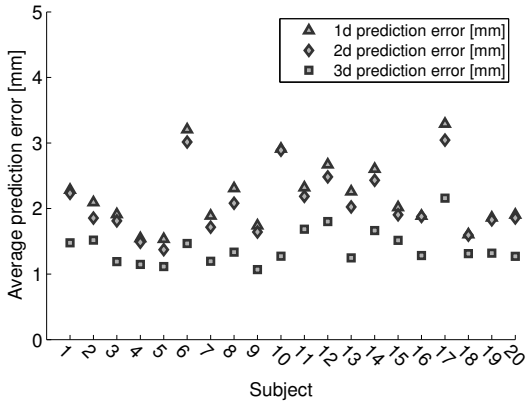

Fig. 7. Average errors for prediction using a single point near the diaphragm in 1D, 2D and 3D.

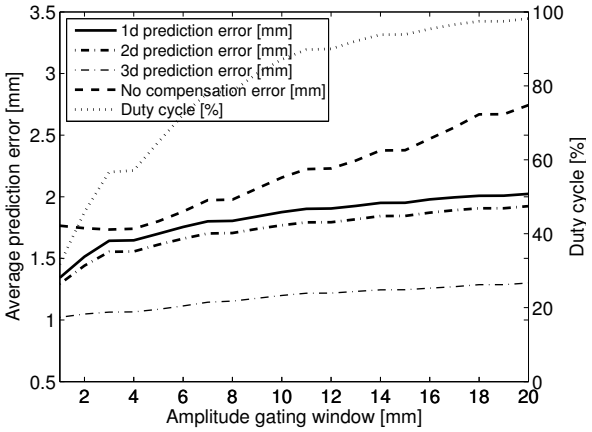

Fig. 8. Comparison of prediction error with amplitude gating. Model-based gating outperforms traditional amplitude gating for any gating window size.

TABLE I

MEDIAN ERROR AND PERCENTILES FOR LEAVE-ONE-OUT EXPERIMENTS OVER 20 min OF RESPIRATION AND $\eta = 2$.

Input	**Median** (mm)	**Percentiles** (mm)		
		$\mathbf{25}^{th}$	$\mathbf{50}^{th}$	$\mathbf{95}^{th}$
1D	2.2	1.7	2.7	3.7
2D	2.1	1.6	2.2	3.5
3D	1.3	0.9	1.4	3.0

Figure 8 depicts results for motion compensation using 1D, 2D and 3D signals (as above) as well as for respiratory gating without compensation. Model-based prediction outperforms gating for any window size. The plot suggests that it is possible to increase the gating window significantly without sacrificing too much accuracy. For example, a gating window of 5 mm results in an average prediction error of 1.8 mm w/o compensation and 1.6 mm in the model-based case. As the gating window is increased to 10 mm, we get an average prediction error of 2.2 mm w/o compensation compared to 1.8 mm (model-based). The error for a 10 mm gating window with model-based motion compensation is thus almost 20% lower than without compensation.

IV. CONCLUSIONS

In this paper we showed how to build statistical motion models and how they can be applied in various realistic scenarios. The prediction power of the motion model was quantitatively evaluated for all scenarios. The results show that organ motion of an unseen subject can be estimated within clinically acceptable margins using a statistical motion model and information from surrogate markers. Additionally, we presented a novel study that compares classical amplitude gating to gating combined with our model-based approach. The results are promising, as they show that our model can improve the accuracy under respiratory gating and can also be used to extend the gating window and thereby reduce treatment times with only a marginal increase in prediction error. In the future work we will use surrogate marker motion data from ultrasound images to predict the tumour location.

ACKNOWLEDGMENT

This work was funded by the Swiss National Science Foundation (SNSF), project CRSII2_127549.

REFERENCES

[1] P. Arnold, F. Preiswerk, B. Fasel, R. Salomir, K. Scheffler, and P. Cattin. Model-based respiratory motion compensation in MRgHIFU. *IPCAI Proceedings*, 2012.

[2] C. B. Barber, D. P. Dobkin, and H. Huhdanpaa. The quickhull algorithm for convex hulls. *ACM T. Math. Software*, 22(4):469–483, 1996.

[3] V. Blanz and T. Vetter. Reconstructing the complete 3D shape of faces from partial information. *Informationstechnik und Technische Informatik*, 44(6):295–302, 2002.

[4] J. Ehrhardt, R. Werner, A. Schmidt-Richberg, and H. Handels. Statistical modeling of 4d respiratory lung motion using diffeomorphic image registration. *Medical Imaging, IEEE Transactions on*, 30(2):251 –265, feb. 2011.

[5] T. He, Z. Xue, W. Xie, and S. T. C. Wong. Online 4-d ct estimation for patient-specific respiratory motion based on real-time breathing signals. In *Proc. MICCAI 2010*, pages 392–399. Springer, 2010.

[6] M. J. Murphy. Tracking moving organs in real time. *Semin. Radiat. Oncol.*, 14(1):91–100, 2004.

[7] F. Preiswerk, P. Arnold, B. Fasel, and P. Cattin. A bayesian framework for estimating respiratory liver motion from sparse measurements. In H. Yoshida, G. Sakas, and M. Linguraru, editors, *Abdominal Imaging. Computational and Clinical Applications*, volume 7029 of *Lecture Notes in Computer Science*, pages 207–214. Springer Berlin / Heidelberg, 2012.

[8] F. Preiswerk, P. Arnold, B. Fasel, and P. C. Cattin. Robust tumour tracking from 2d imaging using a population-based statistical motion model. In *Mathematical Methods in Biomedical Image Analysis (MMBIA), 2012 IEEE Workshop on*, pages 209 –214, jan. 2012.

[9] D. Rueckert, L. I. Sonoda, C. Hayes, D. L. G. Hill, M. O. Leach, and D. J. Hawkes. Nonrigid registration using free-form deformations: application to breast MR images. *IEEE T. Med. Imag.*, 18(8):712–721, 1999.

[10] H. Shirato, Y. Seppenwoolde, K. Kitamura, R. Onimura, and S. Shimizu. Intrafractional tumor motion: lung and liver. *Semin. Radiat. Oncol.*, 14(1):10–18, 2004.

[11] M. von Siebenthal, P. Cattin, U. Gamper, A. Lomax, and G. Székely. 4D MR imaging using internal respiratory gating. In *Proc. MICCAI 2005*, volume 3750 of *LNCS*, pages 336–343. Springer, 2005.

[12] M. von Siebenthal, G. Székely, A. Lomax, and P. Cattin. Systematic errors in respiratory gating due to intrafraction deformations of the liver. *Med. Phys.*, 34(9):3620–3629, 2007.